Microgravity Science and Technology (2022) 34:106
https://doi.org/10.1007/s12217-022-10024-x

RESEARCH

Profiles of Liquid on the Surface of Revolution with Varying Cross-section under Microgravity

Shangtong Chen[1] · Di Wu[2,3] · Yong Li[1] · Jintao Liu[1] · Li Duan[2,3] · Wen Li[1]

Received: 14 August 2022 / Accepted: 30 November 2022 / Published online: 12 December 2022

Abstract

Propellant tanks of satellites usually contain cylindrical structures. Under microgravity, liquid can spread on the revolution's surface regardless of its size. This study focuses on liquid–gas interfaces on the surface of revolution under microgravity. Expressions of profiles of the liquid at equilibrium are proposed in this paper. The profiles have two cases according to the liquid contact angle and the geometry of the revolution. For given liquid contact angle and geometry of the revolution, the profile and volume of the liquid can be obtained by using the Shooting method with certain inputs. Numerical simulation is carried out with the Volume of Fluid method and the numerical results are in good agreement with theoretical predictions. Besides, dimensionless theoretical solutions of the profiles are proposed and the effects of the liquid contact angle and the geometry of the revolution on the profile of the liquid are analyzed in detail.

Keywords Liquid · Profile · Revolution · Microgravity · Shooting method

Introduction

Propellant tanks of satellites usually contain cylindrical structures. In space, liquid can spread on the surface of the revolution regardless of its size due to the absence of gravity, which can affect the efficiency of propellant utilization. Therefore, it is important to study profiles of the liquid on the surface of revolution under microgravity.

Since the well-known Lucas-Washburn equation was derived (Lucas 1918; Washburn 1921), capillary driven flows have attracted much attention and plenty of achievements have been obtained. Capillary driven flows in cylindrical tubes (Levine et al. 1976; Stange et al. 2003; Figliuzzi and Buie 2013; Ramakrishnan et al. 2019; Lei et al. 2021; Bahrini et al. 2022), complex containers (Daniel et al. 2010), axisymmetric geometries (Chassagne et al. 2019), oval tubes (Chen et al. 2021a) and concentric annuli (Chen et al. 2022a) were deeply analyzed and dynamic equations of flows were derived. Weislogel et al. explored capillary driven flows in corners comprehensively and proposed theoretical expressions of flows (1998, 2003, 2005, 2011, 2012, 2018). Capillary rise of liquid in corners with different geometry or wettability was also deeply analyzed and mathematical models describing the liquid flow distance were proposed (Chen et al. 2006; Li et al. 2015; Wu et al. 2018; Tian et al.2019; Zhou and Doi 2020; McCraney et al. 2022). Capillary driven flows between plates were explored and differential equations of meniscus height vs time were presented (Dreyer et al. 1994; Chen et al. 2022b, c). Theories of capillary driven flows and numerical simulations have been used to optimize propellant management devices and analyze liquid behaviours in tanks under microgravity (Li et al. 2020; Zhang et al. 2020; Chen et al. 2019, 2021a, b; Wang et al. 2022). The problem of liquid sloshing under microgravity and aerospace applications were also deeply analyzed (Ibrahim 2001). The sloshing of magnetic liquids in microgravity and the application in space propulsion were discussed by Romero-Calvo et al. (2020, 2021). Thermocapillary-driven dynamics of a free surface in microgravity was studied by Gligor et al. (2022a, b) and measures of control of sloshing were presented. And more generally, a review on fluid control in microgravity was completed by Porter et al. (2021).

✉ Wen Li
gradylee@126.com

[1] Beijing Institute of Control Engineering, China Academy of Space Technology, Beijing 100094, China

[2] Institute of Mechanics, Chinese Academy of Sciences, Beijing 100190, China

[3] College of Engineering and Science, University of Chinese Academy of Sciences, Beijing 100049, China

Since the liquid free surfaces at equilibrium in corners and containers were analyzed and the Concus-Finn condition was presented (Concus and Finn 1974), static capillary surfaces have been paid much attention. Liquid drops and bridges were widely explored and their profiles were obtained (Carroll 1976; Michielsen et al. 2011; Du et al. 2010, 2011; Mason and Clark 1965; Clark et al. 1968; Fortes 1982; Weislogel and Lichter 1996; Gennes et al. 2004; Rabinovich et al. 2005; Vagharchakian et al. 2009; Alexandrou et al. 2010; Honschoten et al. 2010; Wang et al. 2013; Timothy and James 2015; Reyssat 2015). And stability and breakup of capillary bridges were also analyzed deeply. Capillary surfaces in cubes (Mittelmann 1993) and polyhedral containers (Langbein 2002) were discussed and different kinds of free surfaces at equilibrium were presented. The hydrodynamic stability of capillary surfaces subject to constraints of volume conservation, contact-line boundary conditions, and the geometry of the supporting surface was comprehensively analyzed by Bostwick and Steen (2015). Capillary breakup of armored liquid filaments was explored by Zou et al. (2017).

However, liquid drops on the surface of revolution with varying cross-section have not been studied yet. And the method based on minimizing the Gibbs free energy proposed before to predict profiles of liquid drops on conical fibers is too complicated (Michielsen et al. 2011). This study focuses on liquid drops on the surface of revolution under microgravity and expressions of profiles of liquid drops at equilibrium are proposed. Moreover, the Shooting method is adopted to predict the profiles and volume of liquid drops based on the theoretical expressions. Numerical simulation by considering different liquid contact angle, different liquid volume and different geometries is carried out with the Volume of Fluid (VOF) method.

Theoretical Derivation

Propulsion systems or liquid management devices in satellites usually contain surfaces of revolution. In the microgravity environment, the liquid can spread on the surface of revolution. The profiles of liquid drops can be divided into three types according to the liquid contact angle and the geometry of the surface of revolution. The contact angle of liquid on the surface of revolution is θ. The angle between the r axis and the tangent of the surface of revolution is α. When $\theta + \alpha = \pi/2$, the profile is a vertical line. When $\theta + \alpha > \pi/2$ or $\theta + \alpha < \pi/2$, the profiles are shown in Fig. 1a and b respectively. The liquid spreads around the surface of the container with varying cross-section. The blue region represents the liquid with a volume of V_l. In Fig. 1a, the profile is convex, while in Fig. 1b, the profile is concave. The z axis is the symmetry axis of the revolution, and the r axis is perpendicular to the z axis. The revolution

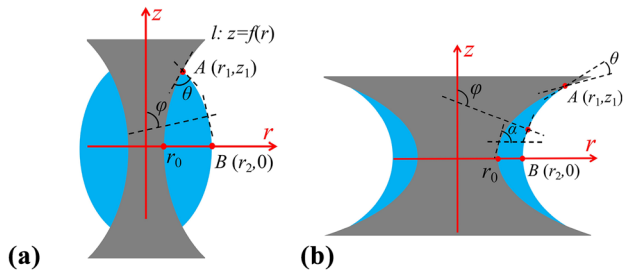

Fig. 1 Cross-sectional view of the model. **a** $\theta + \alpha > \pi/2$. **b** $\theta + \alpha < \pi/2$

is symmetric with respect to both of the z and r axes, so the theoretical analysis is conducted in the first quadrant of the model. φ is the angle between the z axis and the normal to the profile boundary. Points A and B are two endpoints of the profile curve in the first quadrant. The revolution's radius is r_0 when $z = 0$. At each point on Curve AB, there are two principal curvatures, k_1 in the radial direction and k_2 in the azimuthal direction, which can be written as follows (Wang et al. 2013).

$$k_1 = -\frac{d}{dr}\frac{dz/dr}{\sqrt{1 + (dz/dr)^2}} \tag{1}$$

$$k_2 = -\frac{1}{r\sqrt{1 + (dz/dr)^2}} \tag{2}$$

Equations (1) and (2) are the general expressions of the curvatures of an arbitrary surface, and they are independent on fluid dynamics equations and boundary conditions.

The basic assumptions for theoretical analysis are listed below:

1. There is no stress acts on the free surface.
2. The flowing process is isothermal.
3. The liquid is Newtonian, incompressible, and homogeneous.
4. There is no slip between the flowing liquid and the walls.

At every point on the liquid–gas interface, the pressure must be the same. Otherwise, the shape of the liquid drop will change to ensure a constant pressure across the interface of the drop. In space, the gravity is less than 10^{-5} g (g is the constant of the gravity on earth). According to the *Bond* number.

$$Bo = \frac{g\Delta\rho L^2}{\sigma} \tag{3}$$

where $\Delta\rho$, L and σ are the density difference between liquid and gas, the characteristic length and the surface tension

respectively, in most cases the *Bond* number is much smaller than 1 and the gravity can be neglected in space. In the absence of gravitational effects, the condition for the equilibrium state of the liquid drop surface is that the pressure across the drop surface is everywhere constant. The pressure across the interface is called the Laplace pressure and is given by the Young–Laplace equation (Carroll 1976)

$$\Delta p = \sigma\left(k_1 + k_2\right) \tag{4}$$

When σ is a constant, adding up the two curvatures leads to the capillary equation

$$\frac{1}{r}\frac{d}{dr}\frac{rdz/dr}{\sqrt{1+(dz/dr)^2}} = \frac{\Delta p}{\sigma} = C_1 \tag{5}$$

where C_1 is a constant and $(\mathrm{d}z/\mathrm{d}r)/[1 + (\mathrm{d}z/\mathrm{d}r)^2]^{0.5}$ equals $r\sin\varphi$.

Multiplying Eq. (2) by r leads to

$$\frac{rdz/dr}{\sqrt{1+(dz/dr)^2}} = \mathrm{r}\sin\phi = \frac{C_1}{2}r^2 + C_2 \tag{6}$$

where C_2 is a constant. C_1 and C_2 can be determined by combining the equation with the boundary conditions,

$$r = r_1,\ \varphi = \pi - (\vartheta + \alpha),\ \alpha = \arctan\dot{f}_{r_1}$$

$$r = r_2,\ \varphi = \pi/2 \tag{7}$$

which are written as

$$C_1 = 2\frac{r_1\sin(\theta+\alpha) - r_2}{r_1^2 - r_2^2}$$

$$C_2 = r_1 r_2\frac{r_1 - r_2\sin(\theta+\alpha)}{r_1^2 - r_2^2} \tag{8}$$

The gradient of the liquid profile curve can be expressed as follows

$$\text{For } \theta+\alpha > \pi/2\ -\frac{dz}{dr} = \tan\varphi = \frac{\sin\varphi}{\left(1-\sin^2\varphi\right)^{0.5}} \tag{9}$$

$$\text{For } \theta+\alpha < \pi/2\ -\frac{dz}{dr} = \tan\varphi = \frac{\sin\varphi}{-\left(1-\sin^2\varphi\right)^{0.5}} \tag{10}$$

In combination with Eqs. (6) and (8), the gradient of the drop's profile, $\mathrm{d}z/\mathrm{d}r$, can be expressed as a function of r. Substitution of the expression of $\sin\varphi$ in Eqs. (9) and (10) followed by expansion gives a numerator including more than 30 terms. After simplification, the following expressions are obtained to replace original ones.

For $\theta + \alpha > \pi/2$

$$-\frac{dz}{dr} = \frac{r^2\left[r_1\sin(\theta+\alpha) - r_2\right] + r_1 r_2\left[r_1 - r_2\sin(\theta+\alpha)\right]}{\left\{r^2\left[r_1\sin(\theta+\alpha) - r_2\right]^2\left(r_2^2 - r^2\right) - r_1^2\left[r_1 - r_2\sin(\theta+\alpha)\right]^2\left(r_2^2 - r^2\right)\right\}^{0.5}} \tag{11}$$

For $\theta + \alpha < \pi/2$

$$\frac{dz}{dr} = \frac{r^2\left[r_1\sin(\theta+\alpha) - r_2\right] + r_1 r_2\left[r_1 - r_2\sin(\theta+\alpha)\right]}{\left\{r^2\left[r_1\sin(\theta+\alpha) - r_2\right]^2\left(r_2^2 - r^2\right) - r_1^2\left[r_1 - r_2\sin(\theta+\alpha)\right]^2\left(r_2^2 - r^2\right)\right\}^{0.5}} \tag{12}$$

Writing

$$a = \left[r_1 - r_2\sin(\theta+\alpha)\right]/\left[r_1\sin(\theta+\alpha) - r_2\right] \tag{13}$$

Equations (11) and (12) can be converted into the form as below,

$$\text{For } \theta+\alpha > \pi/2\ -\frac{dz}{dr} = \frac{r^2 + ar_1 r_2}{\left[\left(r_2^2 - r^2\right)\left(r^2 - a^2 r_1^2\right)\right]^{0.5}} \tag{14}$$

$$\text{For } \theta+\alpha < \pi/2\ \frac{dz}{dr} = \frac{r^2 + ar_1 r_2}{\left[\left(r_2^2 - r^2\right)\left(r^2 - a^2 r_1^2\right)\right]^{0.5}} \tag{15}$$

Equations (14) and (15) can be solved numerically with the ode45 method if r_1 and r_2 are both known.

The volume of liquid is expressed as

$$V_I = 2\left(V_{AB} - V_C\right) \tag{16}$$

where V_l is the volume of liquid, V_C is the volume of the revolution with a height of z_1 and V_{AB} is the volume surrounded by the liquid profile boundary (Curve AB). Their expressions are listed as follows

$$\text{For } \theta+\alpha > \pi/2\ V_{AB} = \pi\int_0^{z_1} r^2 dz = -\pi\int_{r_2}^{r_1} r^2\frac{r^2 + ar_1 r_2}{\left[\left(r_2^2 - r^2\right)\left(r^2 - a^2 r_1^2\right)\right]^{0.5}}dr \tag{17}$$

$$\text{For } \theta+\alpha < \pi/2\ V_{AB} = \pi\int_0^{z_1} r^2 dz = \pi\int_{r_2}^{r_1} r^2\frac{r^2 + ar_1 r_2}{\left[\left(r_2^2 - r^2\right)\left(r^2 - a^2 r_1^2\right)\right]^{0.5}}dr \tag{18}$$

$$V_c = \pi\int_0^{z_1} r^2 dz \tag{19}$$

Using r_0 to nondimensionalize Eq. (7) leads to

$$\text{For } \theta+\alpha > \pi/2\ -\frac{d\bar{z}}{d\bar{r}} = \frac{\bar{r}^2 + \bar{a}\bar{r}_1\bar{r}_2}{\left[\left(\bar{r}_2^2 - \bar{r}^2\right)\left(\bar{r}^2 - \bar{a}^2\bar{r}_1^2\right)\right]^{0.5}} \tag{20}$$

$$\text{For } \theta+\alpha < \pi/2\ \frac{d\bar{z}}{d\bar{r}} = \frac{\bar{r}^2 + \bar{a}\bar{r}_1\bar{r}_2}{\left[\left(\bar{r}_2^2 - \bar{r}^2\right)\left(\bar{r}^2 - \bar{a}^2\bar{r}_1^2\right)\right]^{0.5}} \tag{21}$$

where $\bar{r}_1 = r_1/r_0, \bar{r}_2 = r_2/r_0, \bar{z}_1 = z_1/r_0, \bar{r} = r/r_0, \bar{z} = z/r_0$ and $\bar{a} = \left[\bar{r}_1 - \bar{r}_2\sin(\theta+\alpha)\right]/\left[\bar{r}_1\sin(\theta+\alpha) - \bar{r}_2\right]$.

Simulation Verification

Mesh models of different kinds of revolution are established. Figure 2 shows a typical mesh model. The fluid domain meshes in three cross-sections are also presented. Grid-independent verification is performed and the total number of grids is designed to be about 1.1 million. Boundary layers are established in the regions close to the surface of the revolution.

Numerical simulation is performed in Fluent with the VOF method. The VOF method can simulate two or more immiscible fluids by solving a single momentum equation and tracking the volume fraction of each fluid in the region. Typical applications include predictions of jet rupture, the movement of large bubbles in liquid, the movement of liquid after dam failure, and the steady-state or transient tracking of any gas–liquid interfaces. Owing to low *Re* numbers during the reorientation process of liquid, the laminar flow is chosen as the flow pattern in the simulation. The time-step size is 0.0005 s. A type of Silicone Oil named by its kinematic viscosity, SO 2, is adopted in our study. Its properties are shown in Table 1.

To reduce simulation time, the liquid is set to be on the middle region of the revolution with a spherical liquid–gas interface in the beginning. As Fig. 3 shows, the yellow surface stands for the liquid–gas interface. The revolution's geometry, the contact angle and the volume of liquid are given. There exists a case that the amount of liquid is not enough to cover the entire circle of the revolution and liquid drops are formed somewhere on the revolution's surface. This case is not considered in our study.

Figure 4a and b show the liquid–gas interfaces at equilibrium when $\theta + \alpha > \pi/2$ while Fig. 4c and d show the liquid–gas interfaces at equilibrium when $\theta + \alpha < \pi/2$. The simulation results are consistent with the results of theoretical analysis. The liquid–gas interfaces are convex when $\theta + \alpha > \pi/2$ and concave when $\theta + \alpha < \pi/2$. The liquid–gas interface is symmetric with respect to the z and r axes. Coordinates of Points A and B can be measured from numerical results. To reduce random errors, final values are obtained by reading coordinate values on two cross sections, and taking the average of these two sets of values for Points A and B respectively. The result data are listed in Table 2 along with the revolution's geometries.

Table 1 Fluid properties (25 °C)

Name	μ (kg/(m*s))	ρ (kg/m^3)	σ (N/m)	ν (10^{-6} m^2/s)
SO 2	0.001746	873	0.0183	2
Air	1.789e-5	1.225	/	1.460e-5

Predictions based on the Shooting Method

With given revolution's geometry and liquid contact angle, when r_1 and r_2 are both known, profiles of the liquid can be obtained through solving Eqs. (14) and (15) with the ode45 method. However, if r_2 or V_l is known, the Shooting method is needed to obtain the profiles. The shooting method is an effective method to solve the two-point boundary value problem of ordinary differential equations. The curve determined by the problem is regarded as the ballistic trajectory, and the solution process is to continuously adjust the test firing conditions to make it reach the

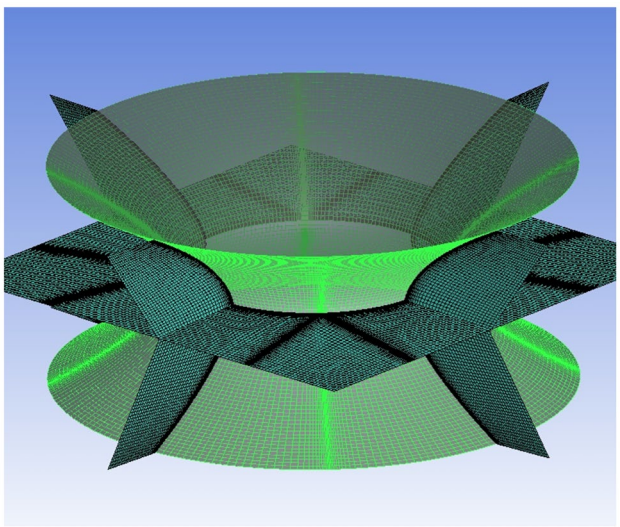

Fig. 2 Typical mesh model established for numerical simulation

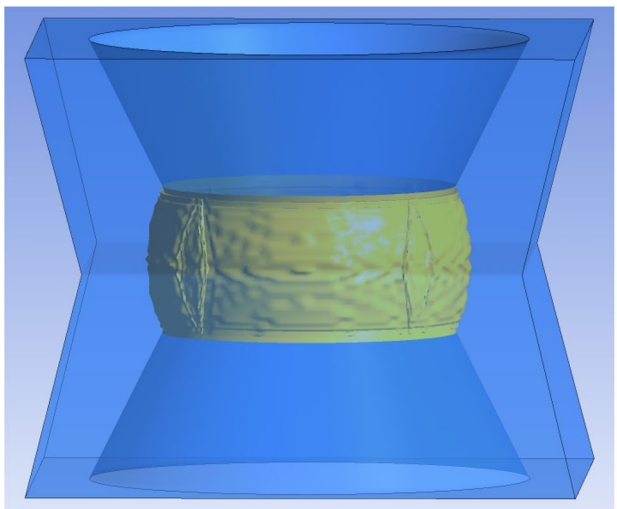

Fig. 3 Initial liquid–gas interface on the surface of a revolution with varying cross-section

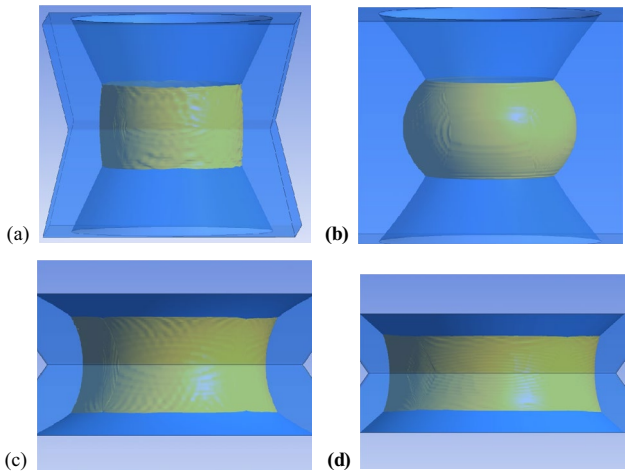

Fig. 4 Liquid–gas interfaces at equilibrium. **a** $r_0 = 40$ mm, $\alpha = 63.44°$, $\theta = 30°$, **b** $r_0 = 20$ mm, $f = 60/30^{0.7}*(r\text{-}20)^{0.7}$, $\theta = 70°$, **c** $r_0 = 10$ mm, $f = 10^{0.5}*(r\text{-}10)^{0.5}$, $\theta = 25°$, **d** $r_0 = 40$ mm, $\alpha = 41.99°$, $\theta = 30°$

predetermined target. The key to this kind of method is to design the steps of selecting the initial value.

When r_2 is known, it is substituted into the mathematical model. Then r_1 is adjusted in a given range until it locates on the revolution's wall. After r_1 is determined through the Shooting method, theoretical predictions of the profile and the volume of liquid can be obtained. In this case, the coordinates of Point B are needed as the inputs. Therefore, this method also relies on numerical simulation. However, it has its unique advantages. For example, when the liquid is spread on the surface of revolution, its volume and interface area are hard to measure directly. But the coordinates of Points A and B on the profile can be easily obtained. Once the coordinates of these points are decided, the volume and interface area can be obtained by using this method.

When V_l is given, it is substituted into the mathematical model at first. Then r_1 is set to be in a given range and r_2 is assigned an estimated value. Calculate the volume of liquid using the guessed values of r_1 and r_2, until the difference between the calculated volume and the given volume is less than $1e^{-5}$. When the calculated volume meets this requirement, the theoretical predictions of the profile are obtained. During this process, r_1 is ensured to be located on the revolution's wall. This method depends on only dozens of lines of codes created according to the theoretical expressions. Numerical simulation is not required in this method. It is easier than the method based on minimizing the Gibbs free energy presented before (Michielsen et al. 2011). With this method, when the geometry of revolution and the volume and contact angle of liquid are known, we can easily predict profiles of liquid drops spreading on the surface of revolution.

Table 2 Model parameters and comparison between numerical and theoretical results

No	Parameters			Numerical results				Theoretical predictions on the premise r_2 is known				Theoretical predictions on the premise V_l is known			
	r_0 [mm]	f [mm]	θ [°]	r_1 [mm]	z_l [mm]	r_2 [mm]	V_l [mm^3]	r_1 [mm]	z_l [mm]	V_l [mm^3]	Ratios of theoretical V_l to numerical ones [%]	r_1 [mm]	z_l [mm]	r_2 [mm]	Ratios of theoretical r_2 to numerical ones [%]
#1	10	$z = 10^{0.5}*(r\text{-}10)^{0.5}$	25	14.68	6.839	12.95	2210	14.87	6.977	2088	94.48	15.00	7.081	13.02	100.5
#2	10	$z = 10^{0.5}*(r\text{-}10)^{0.5}$	30	14.42	6.647	13.07	2210	14.51	6.718	2095	94.80	14.67	6.831	13.17	100.8
#3	10	$z = 10^{0.5}*(r\text{-}10)^{0.5}$	40	13.90	6.237	13.27	2210	13.91	6.251	2071	93.71	14.08	6.386	13.39	97.81
#4	10	$z = 10^{0.5}*(r\text{-}10)^{0.5}$	60	13.10	5.555	13.69	2210	13.10	5.572	2084	94.30	13.24	5.692	13.81	100.9
#5	20	$z = 3(r\text{-}20)$	30	28.77	26.28	33.05	68989	29.87	29.60	73119	106.0	29.62	28.86	32.72	99.00
#6	20	$z = 3(r\text{-}20)$	50	27.34	22.00	34.28	68989	27.69	23.06	67157	97.34	27.78	23.33	34.45	100.5
#7	20	$z = 60/30^{0.7}*(r\text{-}20)^{0.7}$	40	32.41	32.30	36.99	131526	33.57	34.43	132650	100.9	33.50	34.31	36.92	99.81
#8	20	$z = 60/30^{0.7}*(r\text{-}20)^{0.7}$	70	29.01	25.81	39.71	131526	29.26	26.35	126262	96.00	29.48	26.80	40.07	100.9
#9	40	$z = 0.9(r\text{-}40)$	30	66.04	23.42	62.42	180764	66.25	23.62	174941	96.78	66.63	23.96	62.74	100.5
#10	40	$z = 0.9(r\text{-}40)$	60	62.17	19.93	64.67	180764	62.53	20.28	181032	100.1	62.52	20.27	64.65	99.97
#11	40	$z = 2(r\text{-}40)$	30	55.74	31.44	57.58	196155	56.56	33.12	191938	97.85	56.72	33.45	57.75	100.3
#12	40	$z = 2(r\text{-}40)$	50	53.44	26.82	59.28	196155	53.62	27.23	187129	95.40	53.91	27.81	59.69	100.7
#13	40	$z = 34/40^{0.6}*(r\text{-}40)^{0.6}$	40	60.50	22.75	57.30	164384	60.68	22.88	157525	95.82	61.18	23.22	57.71	100.7
#14	40	$z = 34/40^{0.6}*(r\text{-}40)^{0.6}$	80	55.57	19.26	60.11	164384	55.56	19.29	159582	97.08	55.85	19.51	60.42	100.5

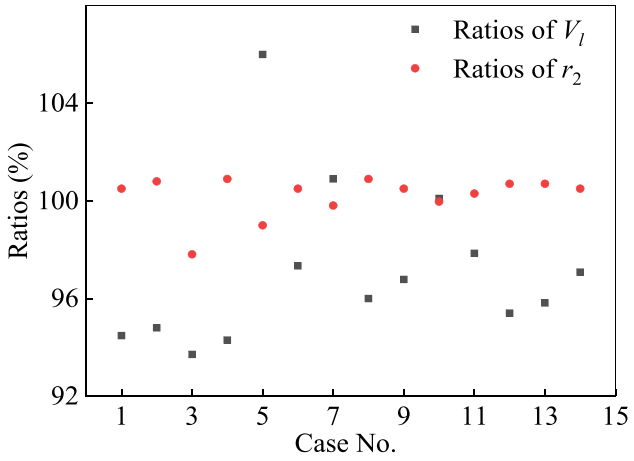

Fig. 5 Ratios of V_l and r_2

Theoretical predictions based on this method are also shown in Table 2. To compare with numerical results more intuitively, ratios of theoretical values of V_l and r_2 to numerical ones are also presented, as shown in Fig. 5. It can be seen that the differences between theoretical predictions and numerical results are mostly within ±5%, which verifies the correctness of the mathematical model and this method.

As shown in Fig. 6a and b, predicted profiles are plotted with numerical results. The black line represents the revolution's wall. The colorful lines stand for predicted profiles under different conditions, while the colorful squares represent numerical data. The condition numbers are labeled at the upper-left corner of the figures. Generally speaking numerical results are in good agreement with predicted profiles. Since the numerical results in Fig. 6a and b is measured from one cross section, and the predicted profiles are based on the average value of r_2 measured from two cross sections, there is a slight difference between the predicted profiles and numerical results, which is acceptable.

Predicted dimensionless results of profiles are shown in Fig. 7a and b. The black lines stand for the revolution's wall and the colorful lines represent profiles of the liquid in the first quadrant with different liquid contact angle. It can be seen that when r_2 is given, the height and volume of the liquid will increase monotonically as the liquid contact angle decreases; when V_l is given, r_2 will decrease monotonically as the liquid contact angle decreases, but the height of the liquid will increase with the decrease of the liquid contact angle. Besides, with the change of the contact angle, profiles of the liquid presents two cases, which is consistent with Fig. 1a and b in the theoretical analysis.

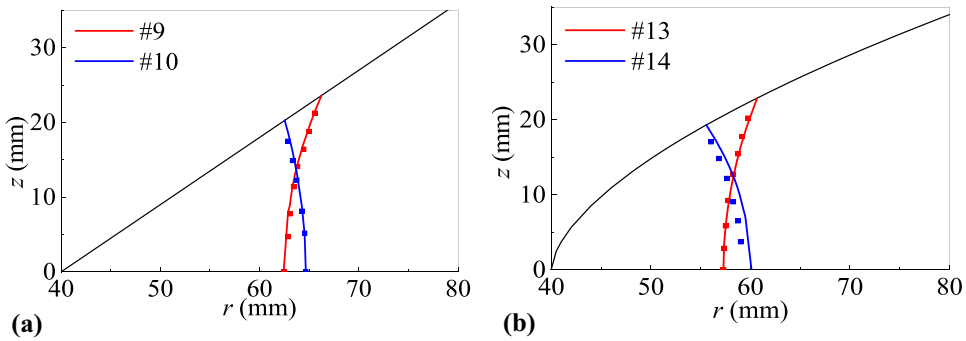

Fig. 6 Predicted profiles vs numerical results. **a** $z = 0.9(r\text{-}40)$ mm and **b** $z = 34/40^{0.6}*(r\text{-}40)^{0.6}$ mm

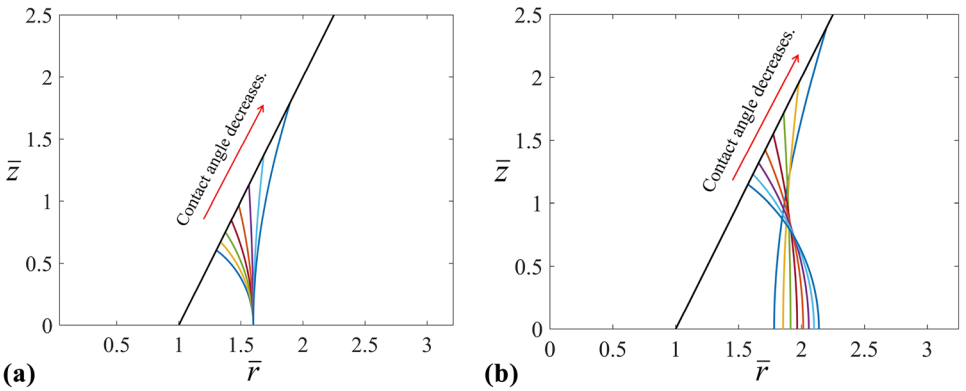

Fig. 7 Predicted dimensionless profiles with the shooting method. **a** $\bar{r}_2 = 1.6$ and the liquid contact angle differs from 10° to 80°. **b** $\bar{V}_l = 16$ and the liquid contact angle differs from 10° to 80°

Conclusions

Profiles of liquid drops on the surface of revolution with varying cross-section under microgravity are obtained through theoretical derivation. The profiles have three cases according to the liquid contact angle and the geometry of the revolution. For given liquid contact angle and geometry of the revolution, if r_1 and r_2 are both known, the profile and volume of liquid drops can be obtained by using the ode45 method. When r_2 or V_l is known, the Shooting method is adopted to predict the profile and volume. Numerical simulation is performed with the VOF method and numerical results are in good agreement with theoretical predictions. Besides, dimensionless expressions of profiles of the liquid are also proposed. For given r_2, the height and volume of the liquid will increase monotonically as the liquid contact angle decreases. And for given V_l, r_2 will decrease monotonically as the liquid contact angle decreases, but the height of the liquid will increase as the liquid contact angle decreases. Understanding capillary phenomena on the surface of revolution will be helpful for liquid management in space, and the mathematical model and the methods to predict the profiles presented in this study can be a theoretical basis for the design of liquid management devices in satellites.

Acknowledgements This research was funded by the Natural Science Foundation Project (No. 12032020).

Authors' Contributions Shangtong Chen wrote the manuscript text. Di Wu and Jintao Liu helped to analyze numerical data. Yong Li, Li Duan and Wen Li offered guidance and support.

Funding This research was funded by the National Natural Science Foundation of China (No. 12032020).

Availability of Data and Material The data of this article can be obtained by contacting the corresponding author.

Declarations

Ethics Approval Not applicable.

Consent to Participate Not applicable.

Consent for Publication Not applicable.

Conflicts of Interest The authors declare no competing financial interest.

References

Alexandrou, A.N., Bazilevskii, A.V., Entov, V.M., Rozhkov, A.N., Sharaf, A.: Breakup of a capillary bridge of suspensions. Fluid. Dyn. **2010**(45), 952–964 (2010)

Bahrini, I., Khemili, F., Abdi Ben Nasrallah, S., Abdelmajid, J.: Study of gas–liquid interface displacement in capillary driven by gas pressurization. Microgravity. Sci. Technol. **34**, 56 (2022)

Bostwick, J.B., Steen, P.H.: Stability of constrained capillary surfaces. Annu. Rev. Fluid. Mech. **47**(1), 539–568 (2015)

Carroll, B.J.: The accurate measurement of contact angle phase contact areas drop volume and Laplace excess pressure in drop on fiber system. J. Colloid. Interface. Sci. **57**(3), 488–494 (1976)

Chassagne, R., Dörflfler, F., Guyenot, M., Harting, J.: Modeling of capillary-driven flows in axisymmetric geometries. Comput. Fluids. **178**, 132–140 (2019)

Chen, S., Han, Z., Duan, L., Kang, Q.: Experimental and numerical study on capillary flow along deflectors in plate surface tension tanks in microgravity environment. AIP. Adv. **9**(2), 025020 (2019)

Chen, S., Ye, Z., Duan, L., Kang, Q.: Capillary driven flow in oval tubes under microgravity. Phys. Fluids. **33**(2), 032111 (2021a)

Chen, S., Duan, L., Kang, Q.: Study on propellant management device in plate surface tension tanks. Acta. Mech. Sin. **37**(10), 1498–1508 (2021b)

Chen, S., Chen, Y., Duan, L., Kang, Q.: Capillary rise of liquid in concentric annuli under microgravity. Microgravity. Sci. Technol. **34**, 30 (2022a)

Chen, S., Wu, D., Wang, J., Duan, L., Kang, Q.: Capillary rise of liquid between plates with a certain angle under microgravity. Chin. J. Theor. Appl. Mech. **54**(2), 326–335 (2022b)

Chen, S., Duan, L., Li, Y., Ding, F., Liu, J., Li, W.: Capillary phenomena between plates from statics to dynamics under microgravity. Microgravity. Sci. Technol. **34**, 70 (2022c)

Chen, Y., Weislogel, M., Nardin, C.: Capillary driven flows along rounded interior corners. J. Fluid. Mech. **556**, 235–271 (2006)

Clark, W.C., Haynes, J.M., Mason, G.: Liquid bridges between a sphere and a plane. Chem. Eng. Sci. **23**, 810–812 (1968)

Concus, P., Finn, R.: On capillary free surfaces in the absence of gravity. Acta. Math. **132**, 177–198 (1974)

Daniel, A.B., Chen, Y., Semerjian, B., Tavan, N., Weislogel, M.M.: Compound capillary flows in complex containers: drop tower test results. Microgravity. Sci. Technol. **22**, 475–485 (2010)

Dreyer, M., Delgado, A., Rath, H.J.: Capillary rise of liquid between parallel plates under microgravity. J. Colloid. Interface. Sci. **163**, 158–168 (1994)

Du, J., Michielsen, S., Lee, H.J.: Profiles of liquid drops at the tips of cylindrical fibers. Langmuir. **26**(20), 16000–16004 (2010)

Du, J., Michielsen, S., Lee, H.J.: Profiles of liquid drops at the bottom of cylindrical fibers standing on flat substrates. Langmuir. **28**(1), 722–728 (2011)

Figliuzzi, B., Buie, C.R.: Rise in optimized capillary channels. J. Fluid. Mech. **731**, 142–161 (2013)

Fortes, M.: Axisymmetric liquid bridges between parallel plates. J. Colloid. Interface. Sci. **88**(2), 338–352 (1982)

Gennes, P., Brochard-Wyart, F., Queré, D., Widom, B.: Capillarity and wetting phenomena: drops, bubbles, pearls, waves. Phys. Today. **57**, 66–67 (2004)

Gligor, D., Salgado Sánchez, P., Porter, J., Tinao, I.: Thermocapillary-driven dynamics of a free surface in microgravity: Response to steady and oscillatory thermal excitation. Phys. Fluids. **34**, 042116 (2022a)

Gligor, D., Salgado Sánchez, P., Porter, J., Ezquerro Navarro, J.M.: Thermocapillary-driven dynamics of a free surface in microgravity: Control of sloshing. Phys. Fluids. **34**, 072109 (2022b)

Honschoten, J.W., Tas, N.R., Elwenspoek, M.: The profile of a capillary liquid bridge between solid surfaces. Am. J. Phys. **78**(3), 277–286 (2010)

Ibrahim, R.A.: Liquid sloshing dynamics with aerospace applications. In: Proceedings of the 9th ASAT Conference, p. 155. Military Technical College in El Cairo, Egypt (2001)

Langbein, D.: Liquid surfaces in polyhedral containers. In: Capillary Surfaces, pp. 213–234. Springer, Berlin, Heidelberg (2002)

Lei, J., Xu, Z., Xin, F., Lu, T.: Dynamics of capillary flow in an undulated tube. Phys. Fluids. **33**(5), 052109 (2021)

Li, Y.Q., Hu, M.Z., Liu, L., Su, Y., Duan, L., Kang, Q.: Study of capillary driven flow in an interior corner of rounded wall under microgravity. Microgravity. Sci. Technol. **27**, 193–205 (2015)

Li, J., Lin, H., Li, K., Zhao, J., Hu, W.: Liquid sloshing in partially filled capsule storage tank undergoing gravity reduction to low/micro-gravity condition. Microgravity. Sci. Technol. **32**, 587–596 (2020)

Lucas, R.: Rate of capillary ascension of liquids. Kolloid. Z. **23**(7), 15–22 (1918)

Levine, S., Reed, P., Watson, E.J., Neale, G.: A theory of the rate of rise of a liquid in a capillary. Colloid. Interface. Sci. **3**, 403–419 (1976)

Mason, G., Clark, W.C.: Liquid bridges between spheres. Chem. Eng. Sci. **20**, 859–866 (1965)

McCraney, J., Weislogel, M.M., Steen, P.: Capillary flow experiments conducted aboard the International Space Station: experiments and simulations. Microgravity. Sci. Technol. **34**, 63 (2022)

Mittelmann, H.D.: Symmetric capillary surfaces in a cube. Math. Comput. Simul. **35**, 139–152 (1993)

Michielsen, S., Zhang, J., Du, J., Lee, H.J.: Gibbs free energy of liquid drops on conical fibers. Langmuir. **27**(19), 11867–11872 (2011)

Porter, J., Salgado Sánchez, P., Shevtsova, V., Yasnou, V.: A review of fluid instabilities and control strategies with applications in microgravity. Math. Model. Nat. Phenom. **16**, 24 (2021)

Ramakrishnan, T.S., Wu, P., Zhang, H., Wasan, D.T.: Dynamics in closed and open capillaries. J. Fluid. Mech. **872**, 5–38 (2019)

Rabinovich, Y.I., Esayanur, M.S., Moudgil, B.M.: Capillary forces between two spheres with a fixed volume liquid bridge: theory and experiment. Langmuir. **21**, 10992–10997 (2005)

Reyssat, E.: Capillary bridges between a plane and a cylindrical wall. J. Fluid. Mech. **773**, R1 (2015)

Romero-Calvo, Á., García-Salcedo, A.J., Garrone, F., Rivoalen, I., Cano-Gómez, G., Castro-Hernández, E., Maggi, F.: StELIUM: A student experiment to investigate the sloshing of magnetic liquids in microgravity. Acta. Astronaut. **173**, 344–355 (2020)

Romero-Calvo, Á., Maggi, F., Schaub, H.: Magnetic positive positioning: Toward the application in space propulsion. Acta. Astronaut. **187**, 348–361 (2021)

Stange, M., Dreyer, M., Rath, H.: Capillary driven flow in circular cylindrical tubes. Phys. Fluids. **15**, 2587–2601 (2003)

Tian, Y., Jiang, Y., Zhou, J.J., Doi, M.: Dynamics of Taylor Rising. Langmuir. **35**, 5183–5190 (2019)

Timothy, F.P., James, B.C.: Asymmetric capillary bridges between contacting spheres. J. Colloid. Interface. Sci. **454**, 192–199 (2015)

Vagharchakian, L., Restagno, F., Leger, L.: Capillary bridgé formation and breakage: a test to characterize antiadhesive surfaces. J. Phys. Chem. B. **113**, 3769–3775 (2009)

Washburn, E.W.: The dynamics of capillary flow. Phys. Rev. **17**, 273–283 (1921)

Weislogel, M.M., Lichter, S.: A spreading drop in an interior corner: theory and experiment. Microgravity. Sci. Technol. **9**, 175–184 (1996)

Weislogel, M.M., Lichter, S.: Capillary flow in an interior corner. J. Fluid. Mech. **373**, 349–378 (1998)

Weislogel, M.M.: Some analytical tools for fluids management in space: isothermal capillary flows along interior corners. Adv. Space. Res. **32**(2), 163–170 (2003)

Weislogel, M.M., Nardin, C.L.: Capillary driven flow along interior corners formed by planar walls of varying wettability. Microgravity. Sci. Technol. **17**(3), 45–55 (2005)

Weislogel, M.M., Baker, J.A., Jenson, R.M.: Quasi-steady capillarity driven flow. J. Fluid. Mech. **685**, 271–305 (2011)

Weislogel, M.M.: Compound capillary rise. J. Fluid. Mech. **709**, 622–647 (2012)

Weislogel, M.M., McCraney, J.T.: The symmetric draining of capillary liquids from containers with interior corners. J. Fluid. Mech. **859**, 902–920 (2018)

Wang, Y., Michielsen, S., Lee, H.J.: Symmetric and asymmetric capillary bridges between a rough surface and a parallel surface. Langmuir. **29**(35), 11028–11037 (2013)

Wang, L., Zhang, X., Yun, Y., Liu, J., Li, W., Huang, B.: Numerical simulation of the reorientation process under different conditions in a vane-type surface tension propellant tank. Microgravity. Sci. Technol. **34**, 37 (2022)

Wu, Z.Y., Huang, Y.Y., Chen, X.Q., Zhang, X.: Capillary driven flows along curved interior corners. Int. J. Multiphase. Flow. **109**, 14–25 (2018)

Zhang, D., Meng, L., Li, Y.: Numerical simulation analysis of liquid transportation in capsule-type vane tank under microgravity. Microgravity. Sci. Technol. **32**, 817–824 (2020)

Zhou, J.J., Doi, M.: Universality of capillary rising in corners. J. Fluid. Mech. **900**, A29 (2020)

Zou, J., Lin, F., Ji, C.: Capillary breakup of armored liquid filaments. Phys. Fluids. **29**(6), 062103 (2017)